Lithium Batteries Hot Paper

How to cite: *Angew. Chem. Int. Ed.* **2021**, *60*, 22812–22817
International Edition: doi.org/10.1002/anie.202107252
German Edition: doi.org/10.1002/ange.202107252

Stabilizing the Solid-Electrolyte Interphase with Polyacrylamide for High-Voltage Aqueous Lithium-Ion Batteries

Xu Hou[+], Rui Wang[+], Xin He, Travis P Pollard,* Xiaokang Ju, Leilei Du, Elie Paillard, Henrich Frielinghaus, Lester C. Barnsley, Oleg Borodin, Kang Xu, Martin Winter, and Jie Li**

Abstract: *The introduction of "water-in-salt" electrolyte (WiSE) concept opens a new horizon to aqueous electrochemistry that is benefited from the formation of a solid-electrolyte interphase (SEI). However, such SEI still faces multiple challenges, including dissolution, mechanical damaging, and incessant reforming, which result in poor cycling stability. Here, we report a polymeric additive, polyacrylamide (PAM) that effectively stabilizes the interphase in WiSE. With the addition of 5 molar % PAM to 21 mol kg^{-1} LiTFSI electrolyte, a $LiMn_2O_4$ || L-TiO_2 full cell exhibits enhanced cycling stability with 86 % capacity retention after 100 cycles at 1 C. The formation mechanism and evolution of PAM-assisted SEI was investigated using operando small angle neutron scattering and density functional theory (DFT) calculations, which reveal that PAM minimizes the presence of free water molecules at the anode/electrolyte interface, accelerates the $TFSI^-$ anion decomposition, and densifies the SEI.*

Introduction

Aqueous lithium-ion batteries (ALIBs) have been receiving intense attention due to their high safety, low cost and low environmental impact compared to their non-aqueous counterparts,[1] which make them attractive for various applications ranging from electronic devices to grid-scale storage system.[2] However, the application of ALIBs is hindered by their low practical voltage and limited number of suitable electrode chemistries that are compatible with the narrow electrochemical stability window (ESW) of the aqueous electrolyte. The new class of highly concentrated aqueous electrolytes, also known as "water-in-salt" electrolyte (WiSE), significantly expands the ESW to ca. 3.0 V via the formation of a solid-electrolyte interphase (SEI).[3] Unfortunately, SEI kinetic stability improvement cannot be only accomplished via increasing salt concentration, especially as water preferentially partitions to the anode interface as anode potential becomes more negative leading to hydrogen evolution in SEI cracks. Such cathodic challenge has essentially restricted the choices of anode materials. Hence, overcoming the cathodic limits of WiSE to allow a wider choice of active materials is key to enabling ALIBs with higher voltage and higher energy density.[4]

It was found that the SEI formed at the anode/electrolyte interface in WiSE mainly consists of a combination of inorganic compounds (LiF, Li_2O and Li_2CO_3) originating from the reduction of dissolved gases (O_2 and CO_2) and the electrolyte salt anion $TFSI^-$.[5] These insoluble salts suppress the H_2 evolution from the reductive decomposition of water. However, the 'real life" SEI in WiSE-based cells is often inhomogeneous with a porous mosaic structure and is susceptible to dissolution, corrosion and mechanical cracking. This allows the ingress of $Li(H_2O)_x^+$ and free water molecules into the porous SEI region and their subsequent reduction.[6]

To further widen the ESW of aqueous electrolytes, extensive efforts were made to increase the salt concentration as well as to tailor salt chemistry, which include approaches via the "water-in-bisalt"[4b] hydrate-melt,[4a] bivalent salts,[7] as well as inert supporting electrolyte, which brought the salt concentration to as high as 63 m.[8] However, the cathodic challenge makes the anion-derived SEI increasingly difficult, while the cost of aqueous electrolyte also increases with the increase of lithium salt concentration, which significantly

[*] Dr. X. Hou,[+] Prof. X. He, Dr. X. Ju, Prof. M. Winter, Prof. J. Li
Helmholtz-Institute Muenster (HI MS), IEK-12, Forschungszentrum Juelich GmbH, Corrensstr. 46, 48149 Muenster (Germany)
Dr. R. Wang,[+] Dr. H. Frielinghaus, Dr. L. C. Barnsley
Jülich Centre for Neutron Science at MLZ, Forschungszentrum Jülich GmbH, Lichtenbergstrasse 1, 85747 Garching (Germany)
Prof. X. He
School of Chemical Engineering, Sichuan University
Chengdu 610065 (China)
E-mail: xinhe@scu.edu.cn
Dr. T. P Pollard, Dr. O. Borodin, Dr. K. Xu
Battery Science Branch, Sensor and Electron Devices Directorate, US Army Research Laboratory, Adelphi, MD 20783 (USA)
E-mail: travis.p.pollard.civ@mail.mil
L. Du, Prof. M. Winter
MEET Battery Research Center, Institute of Physical Chemistry, University of Muenster, Corrensstr. 46, 48149 Muenster (Germany)
Prof. E. Paillard, Prof. J. Li
Department of Energy, Politecnico di Milano
Via Lambruschini 4, 20156 Milano (Italy)
E-mail: jie1.li@polimi.it
Dr. L. C. Barnsley
Australian Synchrotron, ANSTO
800 Blackburn Rd, Clayton 3168 (Australia)
[+] These authors contributed equally to this work.
Supporting information and the ORCID identification number(s) for the author(s) of this article can be found under: https://doi.org/10.1002/anie.202107252.

erodes the commercial potential of such approaches.[9] Hence, it is critical to find an alternative and sustainable pathway to achieve an effective SEI that ensures the sufficient ESW of an aqueous electrolyte.

It is established knowledge that the chemically adsorbed polyacrylamide (PAM) on metal surfaces can shield them against the attack from H^+, and PAM has been widely used as an effective corrosion inhibitor in metal protection technology.[10] Inspired by this knowledge, we apply PAM as a polymeric additive in WiSE in attempt to stabilize the anode/electrolyte interface. Since the polymer is not ionic and does not carry a formal charge, its presence at the anode surface would easily circumvent the cathodic challenge when anions are repelled from and Li^+ is enriching the anode surface.

Results and Discussion

The molecular interactions between PAM and H_2O in WiSE-P_x (P denotes PAM and x denotes its molar percentage) electrolytes were investigated using attenuated total reflection Fourier transform infrared spectroscopy (ATR-FTIR) (Figure 1 a,b). The shifts of C=O stretching mode from 1657 cm^{-1} (pure PAM) to 1690 cm^{-1} and H–N stretching mode from 3,190 cm^{-1} (pure PAM) to 3385 cm^{-1} due to polarization by Li^+ support that a PAM-containing Li^+ solvation sheath is formed. Moreover, the peak at 3250 cm^{-1} arising from H–O stretching mode of water molecules in hydrogen bonding network demonstrates the existence of "free water molecules", which are not participating in Li^+-solvation. Meanwhile, those participating in the solvation of Li^+ is positioned at 3555, and 3620 cm^{-1}.[6] Upon PAM addition, the intensity decreases for both two peaks corresponding to multimer and intermediately-coordinating water, but for the peak representing hydrogen bonding network water we only saw a slight increase. Those observations demonstrate that a small fraction of hydration water in WiSE converts from "bonded" water to network water that is not bound to Li^+ as result of the PAM presence. Thus, water molecules are partially displaced by PAM from the primary solvation sheath of Li^+. This new Li^+ solvation sheath would lead to a local polymer-rich environment when the solvated Li^+ adsorb on the negative electrode surface, which influences the SEI formation chemistry.

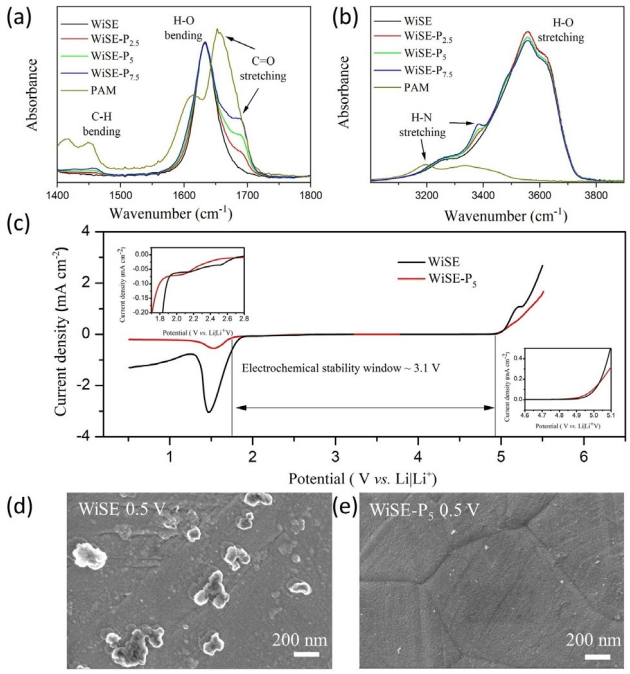

Figure 1. ATR-FTIR absorbance spectra of a series of WiSE-P_x electrolytes (x = 0, 2.5, 5, 7.5) and PAM with wavenumber ranging from (a) 1400–1800 cm^{-1} and (b) 3000 to 3900 cm^{-1}. c) LSV curves of WiSE and WiSE-P_5 based on stainless steel electrodes at a scanning rate of 0.2 $mV s^{-1}$ from OCV to 0.5 V or 5.5 V (vs. $Li|Li^+$). Inserts are the magnified view of the regions near anodic and cathodic potential extremes in the LSV curves. d,e) SEM images of stainless-steel working electrodes after LSV measurements scanning to 0.5 V in WiSE (d) and WiSE-P_5 (e).

The thermal behavior of the WiSE-P_x electrolytes was characterized using DSC (Figure S1). With the addition of PAM, the liquidus transition temperature (T_L) is reduced, suppressing the crystallization of WiSE around room temperature. However, as displayed in Table S1, viscosity also increases while ionic conductivity suffers a corresponding drop due to the addition of PAM. Therefore, as compromise to balance the considerations of the service temperature-range, a PAM-derived interphase and ion transport in bulk, WiSE-P_5 is chosen as the target electrolyte for further electrochemical measurements, which combines the lowest T_L and acceptable ionic conductivity.

The ESW of WiSE and WiSE-P_5 were evaluated by LSV on stainless-steel electrodes. WiSE-P_5 displays an expanded ESW of 3.1 V (from 1.8 V to 4.9 V, vs. $Li|Li^+$, Figure 1 c), which is slightly wider than the parent WiSE (~3.0 V vs. $Li|Li^+$). When scanning to low potential, the cathodic current first increases with a small slope related to hydrogen evolution reaction of free water and $TFSI^-$ decomposition. Then it increases sharply, which is related to the hydrogen evolution from the reduction of coordinating water and further $TFSI^-$ decomposition. Due to the evolution of a protective layer on the surface of the working electrode, the cathodic current decreases, creating a cathodic peak at 1.53 V vs. $Li|Li^+$. On the anodic side, the addition of PAM does not cause obvious change on the onset potential of oxygen evolution, i.e., at 4.9 V vs. $Li|Li^+$ for both cases. However, the gentler slope for the WiSE-P_5 electrolyte suggests that the oxygen evolution reaction on the surface is further suppressed due to the polymer adsorption on the electrode surface. The SEM images of the stainless-steel electrodes after cathodic LSV measurements are shown in Figure 1 d,e. Aggregated particles with the size of $\approx$200 nm are generated and scatter on the surface of electrode in WiSE (Figure 1 d), while WiSE-P_5 introduces a visible layer that homogenously covers the electrode surface (Figure 1 e).

To understand the morphological evolution of SEI formation upon addition of PAM, operando SANS was applied with the cell configuration illustrated in Figure 2 a. During scanning to low or high potential, a quadratic shape of neutron beam is impinging on the cell perpendicularly while

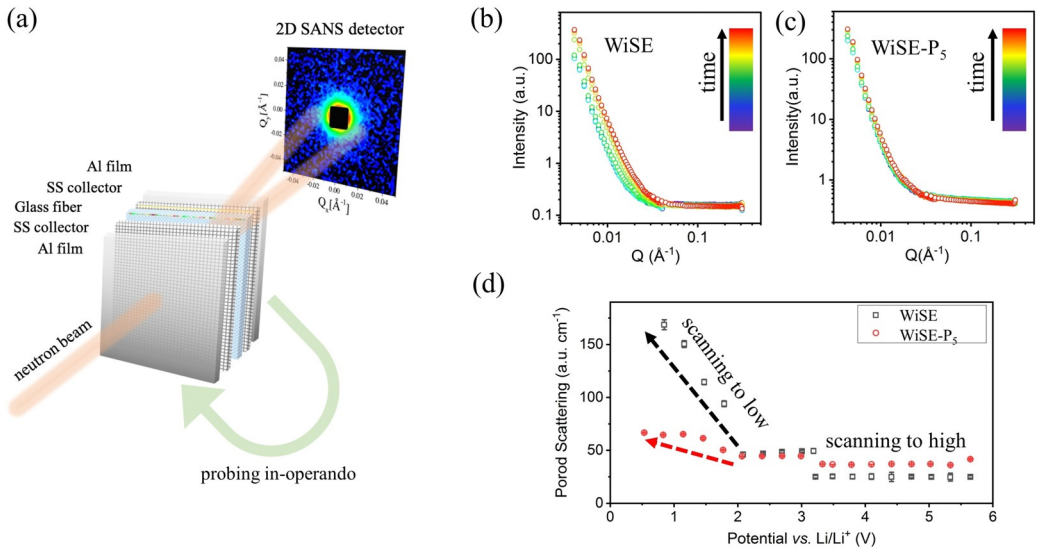

Figure 2. a) Schematic illustration of the operando SANS experiments. Scatter plots along with LSV measurements of cells (b) with WiSE and (c) with WiSE-P_5 when scanning to low potential. d) Porod scattering amplitudes of cells with WiSE and WiSE-P_5 when scanning to different potentials.

the scattered neutrons are captured in a two-dimensional detector, which indicates the structural evolution in real-time. The obtained scattering intensity plots during scanning to low potential or high potential are shown in Figure 2b,c and Figure S2. The morphological dimensions are determined by fitting the scattering data with Porod's law (details in Supporting Information) and using a spherical shape form factor, which correspond to the micrometer scale surface of the electrode and the nanometer roughness. When scanning to high potentials, Porod scattering amplitudes are revealed to keep constant values in both electrolytes, which indicates that no notable morphological changes happen at the electrode surface regardless of whether the PAM additive is used (Figure 2d). However, when scanning to low potentials, the behaviors of these two electrolytes diverge. While the Porod scattering amplitudes in WiSE are first steady until 2.0 V vs. Li | Li$^+$ in WiSE, followed by a drastic increase up to 168 cm^{-1} when further scanning to 0.8 V vs. Li | Li$^+$, the morphological evolution in WiSE-P_5 is less pronounced and the scattering amplitude becomes relatively constant below 1.5 V vs. Li | Li$^+$ with values of ≈65 cm^{-1}. This indicates that below 2.0 V vs. Li | Li$^+$ in WiSE, there is a continuous surface buildup due to sustained decomposition of the electrolyte, which is required to repair the SEI due to its constant dissolution. However, in the WiSE-P_5 electrolyte, morphological changes due to film formation are confined to a narrow potential range of 2.0–1.5 V vs. Li | Li$^+$, beyond which the interphase stabilizes and the parasitic reactions are minimized. The steady scattering amplitude at lower potentials indicates that the anode/electrolyte interface shows an improved stabilization due to addition of PAM. Next, we investigate if cathode stability improvements are due to mere adsorption of PAM or PAM is actively involved in SEI formation and changes its chemistry and properties.

To investigate how PAM interacts with the electrode surface, XPS was conducted on stainless-steel working electrode after LSV measurements in two electrolytes (Figure 3). The peaks in F 1s spectra (Figure 3a,e) are assigned to organic fluorine (688.6 eV) and LiF (685.8 eV), both coming from the TFSI$^-$ anion reduction. Other reduction products of TFSI$^-$ anion, including the sulfur-based species (R-S-N-S species) and Li_2SO_x, are also observed in the N 1s (399.6 eV) and S 2p (170.1 and 169.2 eV) spectra, S 2p (168.0 and 167.3 eV) spectra, respectively. In the presence of PAM additive, higher abundance of inorganic LiF and Li_2S_n are

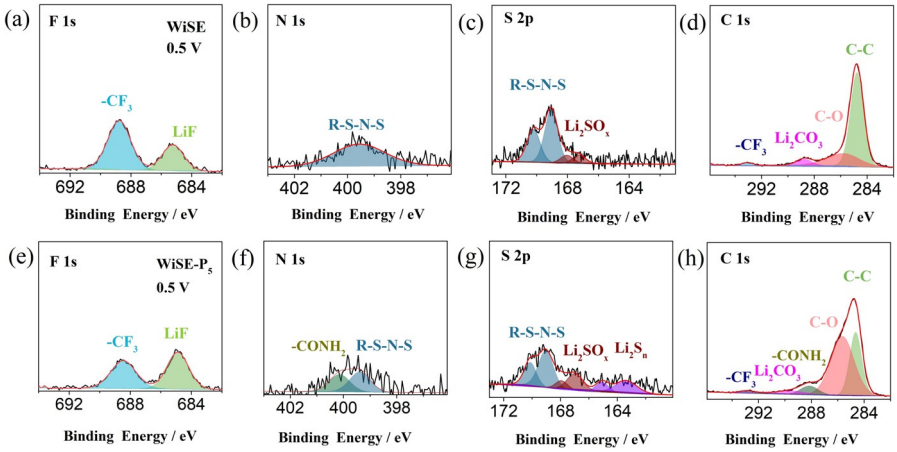

Figure 3. XPS patterns of stainless-steel working electrode after scanning to 0.5 V in WiSE (a–d) and WiSE-P_5 (e–h). (a, e) F 1s, (b, f) N 1s, (c, g) S 2p, (d, h) C 1s.

observed in F 1s spectra (685.8 eV) and S 2p spectra (164.5 and 163.3 eV), respectively. Meanwhile, both C 1s and N 1s spectra reveal the fragments of PAM (-$CONH_2$), as represented by 288.0 eV and 400.2 eV, respectively, indicating that PAM also contributes to SEI, but the extent of its contribution seems to be limited due to the low abundance of -$CONH_2$. This chemistry is due to the partial replacement of water by PAM in the Li^+ solvation sheath, which then brings PAM to the inner Helmholtz layer near the anode surface, where the PAM breaks down. Interestingly, the presence of PAM, either in Li^+-solvation sheath or in the inner Helmholtz layer near the electrode surface, apparently promotes the formation of inorganic fluorides, which were identified as a major SEI components.

DFT calculations (details in Suporting Information) were performed with the focus on understanding of the interaction between PAM with $TFSI^-$ and their reduction potentials. Figures 4 a,b demonstrates the effects of the formation of ion aggregates on the reduction potential of TFSI-derived fragments. Upon formation of Li_xTFSI where $x > 1$, a dramatic increase in the reduction potential is observed indicaing the importance of high salt concentration for inducing the $TFSI^-$ anion decomposition at high potentials. Importantly, the presence of PAM leads to higher reduction potential compared to pure WiSE, generating precursors for sulfides and other downstream products observed in XPS. Reduction potentials for the model WiSE cluster $Li_2TFSI(H_2O)$ are slightly lower (1.7–1.8 V vs. $Li|Li^+$), as shown in Figure S3 and References [3a] and [11]. The presence of PAM on the electrode surface also reduces the prevalence of HER. The reduction of PAM, however, is predicted from DFT (Figure S4) to occur at much lower potentials. At 1.05 V vs. $Li|Li^+$, an urea analogue is predicted to form resulting from the attack of an isocynanic acid intermediate on a neighboring carbamoyl group. Water penetration into the SEI at low potentials may hydrolyze these residues and generate free urea. Near the 0.5 V vs. $Li|Li^+$ cutoff potential, DFT predicts a second reduction mechanism for PAM involving the formation of LiOCN. The acidified carbamoyl group may also be hydrolyzed to form acrylate residues.[12] Isocyanic acid and cyanate group containing additives have been noted previously as promising film-forming species on both negative and positive electrodes.[13] Additionally, Li_2CO_3 from the reduction of dissolved O_2 and CO_2 is observed in C 1s (289.5 eV) with both electrolytes. In summary, it can be concluded that PAM participates in the formation of the SEI in addition to LiF, Li_2CO_3, and sulfur-based species.

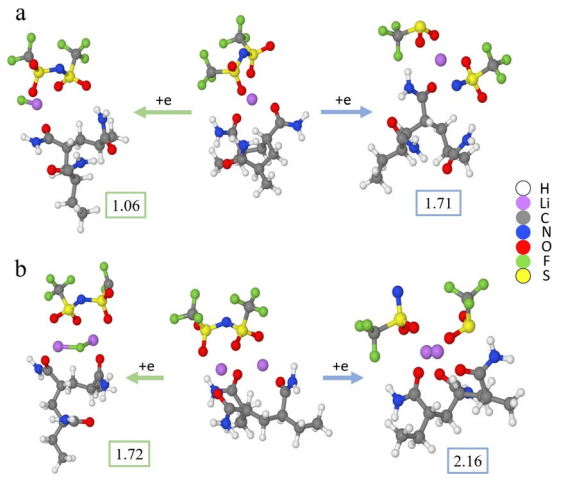

Figure 4. a) Reduction potentials (in Volts) vs. $Li|Li^+$ of LiTFSI-PAM with the SMD(acetone)/M052X/6–31 + G(d,p) model chemistry highlighting defluorination (left) and S–N cleavage (right). b) Reduction potentials vs. $Li|Li^+$ of Li_2TFSI-PAM (simulating salt aggregation) with the SMD(acetone)/M052X/6–31 + G(d,p) model chemistry highlighting defluorination (left) and S–N cleavage (right).

To understand the morphological evolution of SEI in different electrolytes, the stainless-steel electrodes removed from cells after cathodic LSV measurement (to 1.9 V vs. $Li|Li^+$) were also examined under SEM. According to the aqueous SEI formation mechanism in WiSE proposed by Bouchal et al., it can be inferred that severe hydrogen evolution reaction occurs alongside precipitation/dissolution of LiTFSI salt and decomposition products.[14] The influx of water from bulk WiSE to the Helmholtz layers near the electrode surface at low potentials is extremely disruptive to the formation process of SEI. As shown in Figure S5, reduction products are scattered on the surface of the electrode in WiSE with uneven distribution because of the competitive reduction of water. On the contrary, a smooth surface can be observed on the electrode surface recovered from WiSE-P_5. With PAM additive in WiSE, the chemical adsorption of PAM reduces the presence of $Li^+(H_2O)_n$ and water on the anode surface even before the interphase formation. When the electrode potential is driven to values below 1.5 V vs. $Li|Li^+$, such PAM-rich electrode surface naturally suppresses hydrogen evolution, and minimizes the dissolution of the SEI when the formation process starts. A schematic illustration of the SEI formation process in WiSE and WiSE-P_5 are displayed in Figure S6. The PAM presence favors the reductive decomposition of TFSI over that of water in this competitive process. As a result, a dense and thin SEI layer is formed with the participation of the PAM additive.

$LiMn_2O_4$ and L-TiO_2 electrodes were used as positive and negative electrodes, respectively, to assemble full cells in order to verify the practical effect of PAM additive. Individual CV measurements on both $LiMn_2O_4$ and L-TiO_2 electrodes were conducted in three-electrode cells with activated carbon as counter electrode and $Ag|AgCl$ as reference electrode in the different electrolytes. The redox peaks of the L-TiO_2 negative electrode can be observed at 2.27 V/2.07 V in WiSE and at 2.28 V/2.06 V in WiSE-P_5 electrolyte in the first cycle, respectively (Figure 5 a). The slightly bigger potential gap between the oxidation and reduction peaks in WiSE-P_5 is attributed to the uncompensated resistance increase arising from the SEI formation. It can be noticed that in WiSE, the oxidation peak moves to a higher potential with a decrease in intensity in the second scan, indicating capacity fading due to hydrogen competing with the buildup of SEI and less protective SEI. While in WiSE-P_5 both changes are weaker and, in particular, the peak intensity stays constant. Thus, the less pronounced hydrogen evolution occurring in WiSE-P_5 predicts higher reversibility of the lithiation/delithiation in L-TiO_2 electrode. These results indicate that an effective SEI

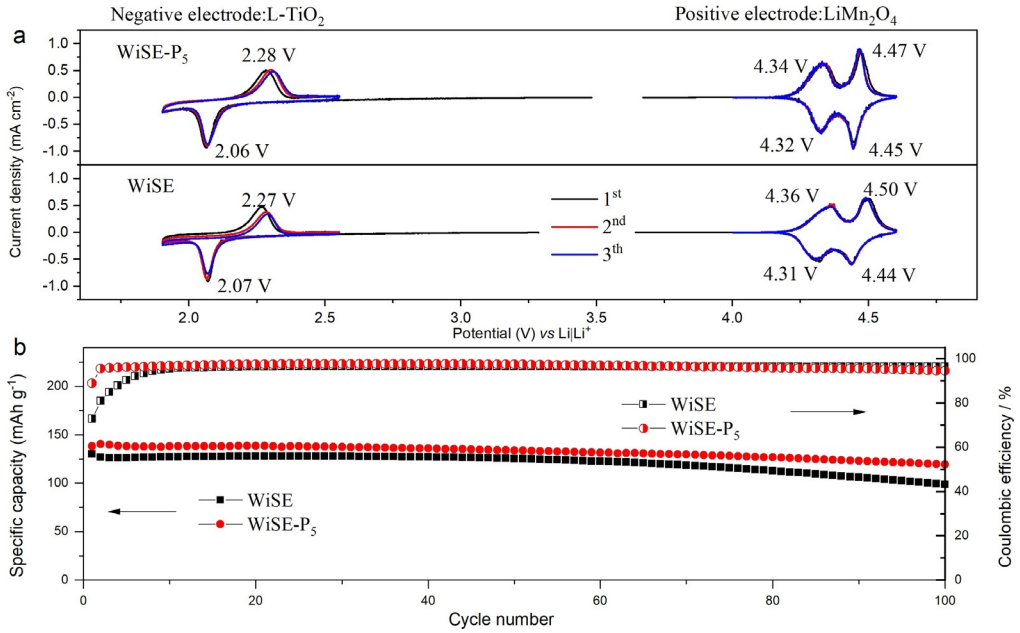

Figure 5. Electrochemical performance of $LiMn_2O_4$ || L-TiO_2 full cells. a) CV results of $LiMn_2O_4$ and L-TiO_2 electrodes in different electrolytes at a scanning rate of 0.1 $mV s^{-1}$. b) The cycle stability and CE of full cell with WiSE electrolyte or WiSE-P_5 electrolyte at 1 C.

can be formed on the surface of L-TiO_2 negative electrode during the initial cycling. Due to the high oxygen evolution potential in "water-in-salt" electrolyte, $LiMn_2O_4$ electrodes show high reversibility in both WiSE and WiSE-P_5. Interestingly, the potential difference of each redox couple in WiSE-P_5 is smaller than those in WiSE and the peak areas proportional to the charge/discharge capacities are larger in WiSE-P_5, demonstrating a faster Li ion transfer at the positive electrode as well.

The galvanostatic performance of $LiMn_2O_4$ || L-TiO_2 full cells in two-electrode coin cell configuration using both WiSE and WiSE-P_5 are shown in Figure 5b. A higher reversible capacity (138 $mAh g^{-1}$, based on the mass of L-TiO_2) is obtained from the cell with WiSE-P_5, as compared to the 130 $mAh g^{-1}$ obtained from the cell with WiSE. The Coulombic efficiency (CE) of cell containing WiSE-P_5 reaches 88.9% in the first cycle, which is much higher than that obtained with WiSE (72.8%). Moreover, the CE of the cell with WiSE-P_5 electrolyte increases to 95.5% in the second cycle and stabilizes during subsequent cycles, while this trend in WiSE occurs much more gradually. After 100 cycles, $LiMn_2O_4$ || L-TiO_2 full cell with WiSE-P_5 is still able to deliver a discharge capacity of 119 $mAh g^{-1}$, which is 86.3% of the initial capacity, a significant enhancement as compared with the capacity retention of 76% achieved in WiSE. This improvement is attributed to the improvements of SEI whose formation is assisted by PAM as electrolyte additive to "water-in-salt" electrolyte.

Conclusion

Polyacrylamide has been introduced to "water-in-salt" electrolyte as an effective electrolyte additive that assists in the formation of a stable SEI. Because of the participation of PAM in the Li^+ primary solvation sheath, a polymer-rich layer is formed by chemical adsorption of PAM on the electrode surface, which not only expels water molecules and $Li^+(H_2O)_n$ from the electrode surface, but also participate in the interphasial chemistry. Consequently, the electrochemical stability window of the aqueous electrolyte is broadened. Benefitted from the PAM-presence, $LiMn_2O_4$ || L-TiO_2 full cell shows a promising cycle stability and faster activation. This new mechanism of interphase assistance provided by a polymeric species can be instructive for the design of new electrolyte and interphase chemistries for the future high-voltage ALIBs.

Acknowledgements

The authors would like to acknowledge financial support from the European Union through the Horizon 2020 framework program for research and innovation within the projects "SPIDER" (814389) and Energy of the State of North Rhine-Westphalia (MWIDE, Germany) within the project "GrEEn" (313-W044A). Modelling work at Army Research Laboratory was supported by the Joint Center for Energy Storage Research, an Energy Innovation Hub funded by the US Department of Energy under cooperative agreement no. W911NF-19-2-0046. Special thanks to Debbie Berghus (University of Münster) for the DSC measurements. Open Access Funding provided by Politecnico di Milano within the CRUI-CARE Agreement.

Conflict of Interest

The authors declare no conflict of interest.

Keywords: "water-in-salt" electrolyte · lithium-ion batteries · small-angle neutron scattering · polymer additive · solid-electrolyte interphase

[1] R. Schmuch, R. Wagner, G. Hörpel, T. Placke, M. Winter, *Nat. Energy* **2018**, *3*, 267 – 278.
[2] a) A. Eftekhari, *Adv. Energy Mater.* **2018**, *8*, 1801156; b) X. Chen, H. Huang, L. Pan, T. Liu, M. Niederberger, *Adv. Mater.* **2019**, *31*, 1904648; c) V. L. Martins, R. M. Torresi, *Curr. Opin. Electrochem.* **2020**, *21*, 62 – 68.
[3] a) L. Suo, O. Borodin, T. Gao, M. Olguin, J. Ho, X. Fan, C. Luo, C. Wang, K. Xu, *Science* **2015**, *350*, 938; b) M. Winter, *Z. Phys. Chem. (Muenchen Ger.)* **2009**, *223*, 1395 – 1406.
[4] a) Y. Yamada, K. Usui, K. Sodeyama, S. Ko, Y. Tateyama, A. Yamada, *Nat. Energy* **2016**, *1*, 16129; b) L. Suo, O. Borodin, W. Sun, X. Fan, C. Yang, F. Wang, T. Gao, Z. Ma, M. Schroeder, A. von Cresce, S. M. Russell, M. Armand, A. Angell, K. Xu, C. Wang, *Angew. Chem. Int. Ed.* **2016**, *55*, 7136 – 7141; *Angew. Chem.* **2016**, *128*, 7252 – 7257.
[5] L. Suo, D. Oh, Y. Lin, Z. Zhuo, O. Borodin, T. Gao, F. Wang, A. Kushima, Z. Wang, H.-C. Kim, *J. Am. Chem. Soc.* **2017**, *139*, 18670 – 18680.
[6] N. Dubouis, P. Lemaire, B. Mirvaux, E. Salager, M. Deschamps, A. Grimaud, *Energy Environ. Sci.* **2018**, *11*, 3491 – 3499.
[7] S. Kondou, E. Nozaki, S. Terada, M. L. Thomas, K. Ueno, Y. Umebayashi, K. Dokko, M. Watanabe, *J. Phys. Chem. C* **2018**, *122*, 20167 – 20175.
[8] L. Chen, J. Zhang, Q. Li, J. Vatamanu, X. Ji, T. P. Pollard, C. Cui, S. Hou, J. Chen, C. Yang, L. Ma, M. S. Ding, M. Garaga, S. Greenbaum, H.-S. Lee, O. Borodin, K. Xu, C. Wang, *ACS Energy Lett.* **2020**, *5*, 968 – 974.
[9] L. Droguet, A. Grimaud, O. Fontaine, J. M. Tarascon, *Adv. Energy Mater.* **2020**, *10*, 2002440.
[10] a) V. Srivastava, S. Banerjee, M. M. Singh, *J. Appl. Polym. Sci.* **2010**, *116*, 810 – 816; b) C. Wang, C. Zou, Y. Cao, *J. Mol. Struct.* **2021**, *1228*, 129737.
[11] H.-G. Steinrueck, C. Cao, M. Lukatskaya, C. Takacs, G. Wan, D. Mackanic, Y. Tsao, J. Zhao, B. Helms, K. Xu, O. Borodin, J. F. Wishart, M. Toney, *Angew. Chem. Int. Ed.* **2020**, *59*, 23180 – 23187; *Angew. Chem.* **2020**, *132*, 23380 – 23387.
[12] M. J. Caulfield, G. G. Qiao, D. H. Solomon, *Chem. Rev.* **2002**, *102*, 3067 – 3084.
[13] a) C. Korepp, W. Kern, E. A. Lanzer, P. R. Raimann, J. O. Besenhard, M. H. Yang, K. C. Möller, D. T. Shieh, M. Winter, *J. Power Sources* **2007**, *174*, 387 – 393; b) P. Dong, D. Wang, Y. Yao, X. Li, Y. Zhang, J. Ru, T. Ren, *J. Power Sources* **2017**, *344*, 111 – 118.
[14] R. Bouchal, Z. Li, C. Bongu, S. Le Vot, R. Berthelot, B. Rotenberg, F. Favier, S. Freunberger, M. Salanne, O. Fontaine, *Angew. Chem. Int. Ed.* **2020**, *59*, 15913 – 15917; *Angew. Chem.* **2020**, *132*, 16047 – 16051.

Manuscript received: May 31, 2021
Accepted manuscript online: August 11, 2021
Version of record online: September 12, 2021

